CHAPTER II

Theoretical Aspects

2.1 Basic concepts of electrochemistry

Electrochemistry deals with the chemical reactions involving transfer of electrons at the interface between an electrode (electronic conductor) and an electrolyte (ionic conductor). Electrochemistry has wide applications in the field of energy conversion and storage systems such as fuel cell, solar cell, batteries, supercapacitors and electrochemical and biochemical sensors etc. [1, 2]. There are two distinct divisions of electrochemistry: first one is 'equilibrium electrochemistry', that occurs upon building up a steady state potential difference between the electrode and electrolyte without flow of a sustained current [3, 4]. 'Dynamic electrochemistry' is another division that corresponds to the study of electron transfer reactions between an electrode and reactant molecules in electrolyte solution and where the current is recorded as a function of voltage applied between the electrode and electrolyte [5]. This plot of current vs. applied voltage is known as voltammogram, which is analysed to obtain the details of electron kinetics in an electrochemical reaction. The transfer of electrons can be categorized into two types: heterogeneous and homogeneous electron transfers. In case of heterogenous electron transfer, the transfer of electrons takes place via an interface; while in homogeneous electron transfer, redox reaction involves with transfer of electrons between two species in the same phase [3]. The electron transfer process at the electrode-electrolyte interface can be explained by the oxidation and reduction reactions as shown below:

$$O + ne \rightleftharpoons R \qquad (2.1)$$

Where O and R are the oxidized and reduced species, respectively and n is the number of electrons transferred during the reaction.

2.1.1 Electrochemical cell

An electrochemical cell comprises two electrodes as depicted in Figure 2.1 (i), the working electrode (WE) and the counter electrode (CE) along with an electrolyte solution. The electrochemical processes at the WE must not be interfered by CE.

Therefore, Platinum, being an inert material, has been used as CE in electrochemical devices. Inside an electrochemical cell, a potential difference is developed at the interface between the electrode and electrolyte, owing to dissimilar chemical potentials of the two species, driving transfer of charges such as electron movement in the electrode and ion transport in the electrolyte to attain an equilibrium condition [3, 5]. Hence, a potential difference is produced at the electrode-electrolyte interface due to charge separation,

$$\Delta E = E_{Electrode} - E_{Electrolyte} \quad (2.2)$$

Since the potential of an ideal WE is not typically constant, therefore it cannot be regarded as reference electrode (RE). Therefore, a standard electrode, consist of constant composition and large input impedance with negligible amount of current flow, is known as RE, which is non-polarizable with a well-defined electrode potential i.e. its potential does not vary upon application of current [6]. Hence, in a three-electrode cell as shown in Figure 2.1 (ii), potential of the WE is monitored with respect to RE and the current is monitored with respect to CE.

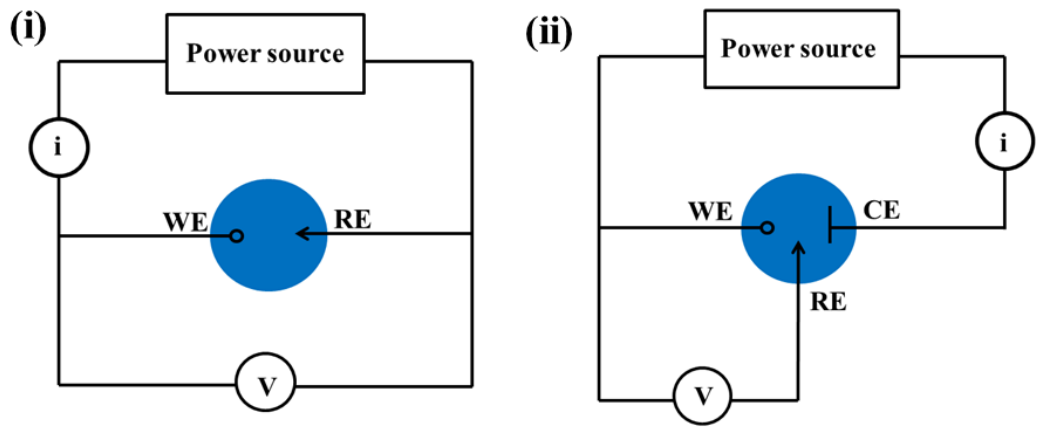

i = Ammeter V = Voltammeter

Figure 2.1: *Schematic diagram of electrochemical cell with (i) two electrode and (ii) three electrode configurations.*

Standard hydrogen electrode (SHE, 0 V) is the internationally accepted primary RE. However, potentials are often measured relative to REs other than SHE, since it is not much suitable from an experimental point of view.

The change in potential at the WE can be measured with respect to RE as shown below [3]:

$$E = \left(E_{Electrode} - E_{Electrolyte}\right) - Constant \quad (2.3)$$

Where, constant is measured by the RE.

The energy of electrons in the electrode can be raised by driving the potential of WE to more negative values so that they can attain a sufficient energy to jump into empty electronic states on a species in the electrolyte, generating electron flow from electrode to electrolyte known as reduction current [7]. Similarly, when more positive potential is applied to the WE, then energy of electrons in the electrode is lowered enough so that the electrons in the electrolyte move to more favourable energy levels on the electrode, thus producing oxidation current.

When the electron transfer kinetics is rapid enough, then equilibrium is attained within a short time period i.e. the rates of oxidation and reduction reactions become same with zero current flow through the circuit. In this case, the potential is dependent on the concentrations of oxidizing and reducing species and it is governed by Nernst Equation [3]:

$$E_{eq} = E_f^0 + \frac{RT}{nF} \ln \frac{C_O^*}{C_R^*} \tag{2.4}$$

Where E_f^0 is the formal potential for half-reaction, which signifies the potential of a redox couple at equilibrium in a system where the concentrations of oxidized and reduced species are one formal, C_O^* and C_R^* are the bulk concentrations of oxidized and reduced species, respectively and other terms have usual meanings.

2.1.2 Faradaic and non-faradaic processes

There are two types of mechanisms, called as faradaic and non-faradaic processes occur at the electrode surface, which can contribute to net current flowing through the electrochemical system. It appears due to exchange of electrons between the electrode and electroactive species in the electrolyte. Either oxidation or reduction of electroactive species can occur based on the direction of movement of electrons [3]. In faradaic process, the extent of chemical reaction depends on the number of electrons pass through the electrode-electrolyte interface. Under certain conditions, a given electrode-electrolyte interface will exhibit a range of potentials where no charge-transfer reaction takes place since these reactions are thermodynamically or kinetically unfavourable. Although, adsorption and desorption of ions at the electrode surface can cause changes in the interfacial structure without altering the potential or composition of electrolyte. This process is termed as non-faradaic process, where charge does not cross the interface, however transient current can flow with change in potential, composition of electrolyte

and the electrode area. Both faradaic and non-faradaic processes take place during electrode reaction contributing to overall current [8]. However, the contributions from non-faradaic processes are minimized using properly designed experimental conditions and only faradaic processes are taken into account.

2.1.3 The electrode and electrolyte interface

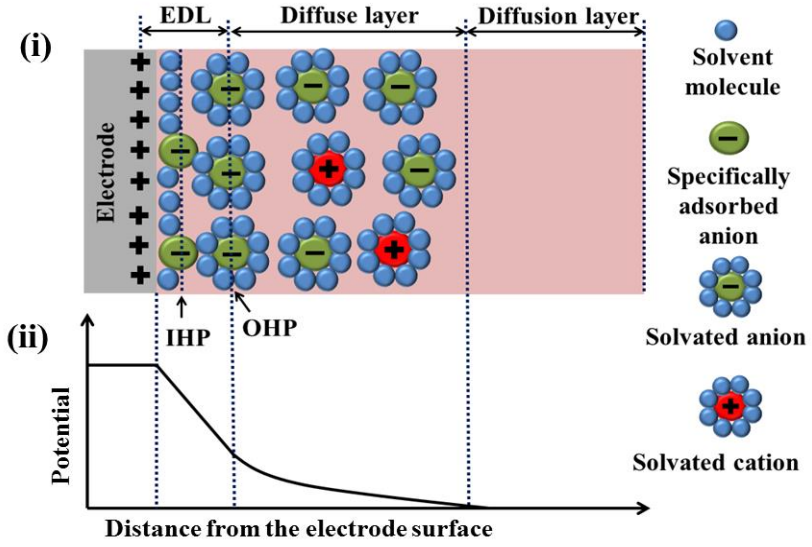

Figure 2.2: *(i) Schematic diagram of an EDL formed outside a positively charged electrode. (ii) The variation of potential across the electrode-electrolyte interface.*

In electrochemical experiment, charge separation occurs between a charged electrode and the electrolyte solution causing a potential difference across the interface. The ions in the nearest vicinity of electrode surface re-orientate themselves in order to attain energetically the most favourable arrangement and to neutralize the interfacial zone. Consequently, oppositely charged ions are attracted to the electrode surface, while the ions with similar charge are repelled from the electrode surface [3]. An electric field is built up at the interfacial region and therefore, this region is named as 'electric double layer (EDL)'. The schematic illustration of EDL is depicted in Figure 2.2 (i). An EDL behaves as a capacitor and the capacitance is termed as double layer capacitor (C_{dl}). The layer adjacent to the electrode surface is termed as inner Helmholtz layer consisting of solvent molecules and specifically adsorbed ions and molecules. The locus of the centres of specifically adsorbed ions is known as inner Helmholtz plane (IHP) [9]. Outside the inner layer, it is outer Helmholtz layer (OHL), containing non-specifically adsorbed

solvated counter ions that interact with the electrode via long-range electrostatic forces. The solvated ions can approach the electrode surface up to a certain distance due to size of the solvated molecules and locus of electrical centres of these closest solvated ions to the electrode surface is termed as outer Helmholtz plane (OHP) [9]. The potential across the EDL interface is linear and steep since the two oppositely charged layers are separated by a small and fixed distance as shown in Figure 2.2 (ii). Another layer, termed as diffuse layer is formed outside the Helmholtz layer, to counteract the charges at electrode surface. This layer is composed of both anions and cations with a large concentration near the OHL but lowering concentration towards the bulk of the electrolyte [10]. There is exponential decay in the potential across the diffuse layer (Figure 2.2 (ii)). When reactant molecules come near to the electrode surface, their electronic energy levels are shifted, thus affecting the electron transfer rate with the electrode. The rate of oxidation and reduction reactions is same in case of equilibrium electrochemistry, which is defined as exchange current. However, in case of dynamic electrochemistry, either oxidation or reduction is dominant and consumption of reactants occurs at the vicinity of electrode surface [7].

2.1.4 Electrode reaction mechanism

The electrochemical reaction mechanism for the transfer of electrons between the oxidized species, O and the reduced species, R is composed of a series of steps as shown in Figure 2.3. The current flowing through the electrode is controlled by the processes such as [3, 8]: (i) Mass transport, i.e. transport of oxidized species O from the bulk solution towards the surface of electrode, (ii) exchange of electrons at the electrode, (iii) Chemical reactions such as homogenous (e.g. protonation) and heterogeneous (e.g. catalytic decomposition) at the vicinity of electrode surface preceding or following the electronic transfer step and (iv) Other surface reactions including adsorption, desorption or crystallization processes. Electrode activities involving electron transfer process can occur in several consecutive steps. The reaction mechanisms at the surface of electrode along with mass transfer of species at the interfacial region between the electrode and bulk solution can affect overall reaction rate. Mass transfer is achieved through three modes [8]: (i) Diffusion: movement of ions under the influence of concentration gradients. (ii) Migration: motion of a charged species in a gradient of electric potential.

(iii) Convection: caused by hydrodynamic transport. The reasons behind convection can be natural (caused by variation in density) or forced (stirring).

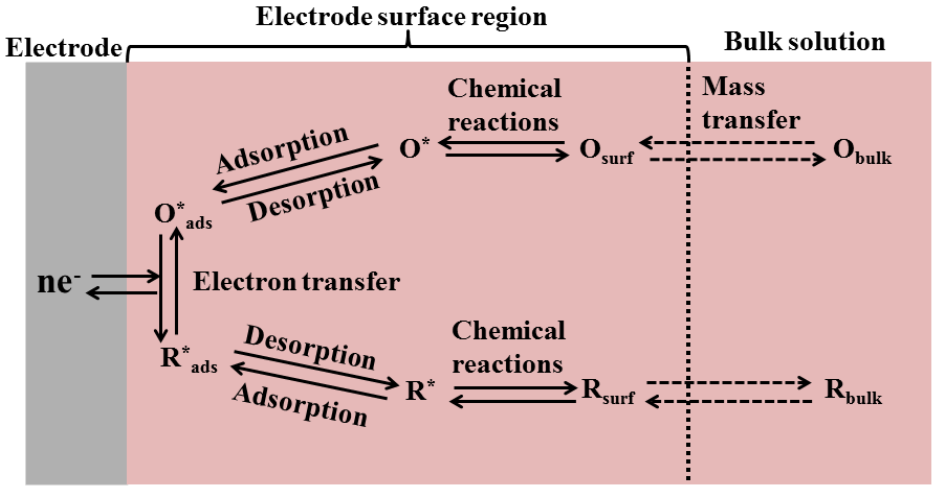

Figure 2.3: *Pathway of a general electrode reaction.*

2.2 Cyclic voltammetry

Cyclic voltammetry (CV) is a widely used electroanalytical technique for investigating the electrochemical behaviour of a system. It was first reported in the year 1938 and theoretical description was given by Randles and Sevcik in 1948 [11, 12]. CV is the preliminary technique used to obtain qualitative information about electrochemical redox reactions such as the thermodynamics of redox reactions, heterogeneous electron transfer kinetics, mass transport activity and adsorption processes. In this technique, a triangular potential waveform (Figure 2.4) is applied to the working electrode that is immersed in an electrolyte solution, resulting into a current-voltage plot, termed as cyclic voltammogram [8, 13].

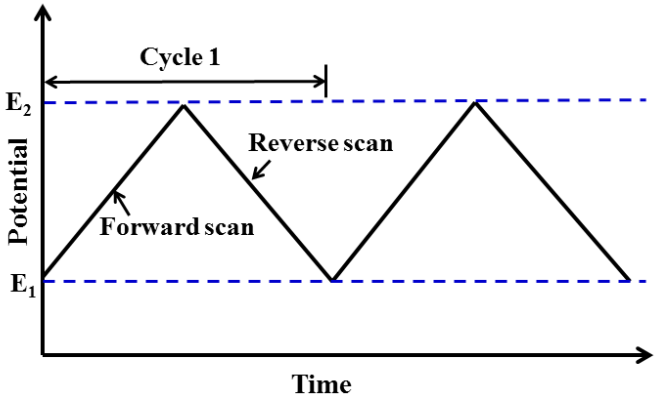

Figure 2.4: *Triangular potential waveform used in cyclic voltammetry showing the variation of potential from an initial value (E_1) to a final value (E_2).*

The applied potential at the working electrode varies from an initial potential E_1, where no redox reaction occurs to a final potential E_2 at a certain sweep or scan rate (Figure 2.4). If the scan is stopped at E_2, the resulting voltammogram is known as linear sweep voltammogram (LSV) (Figure 2.5 (i)). However, by reversing the scan back to potential E_1 from E_2 at a same sweep rate, a cyclic voltammogram (Figure 2.5 (ii)) is obtained. During change in potential, one or more redox processes take place in the electrolyte solution giving rise to faradaic current. At point A of Figure 2.5 (ii), there is no conversion from the reduced form, R to the oxidised form, O since the initially applied potential is not sufficient to induce any electron transfer [14]. With increase in potential, R is gradually converted into O causing concentration gradients for both R and O. Therefore, the anodic current rises exponentially with potential and reaches to the point B, where the applied potential is positive enough to instantaneously oxidize any R over the electrode surface to O. A depletion layer is formed at the electrode and electrolyte interface due to formation of large number of O [15]. Hence, the value of current is governed by rate of mass transport to the surface of electrode and therefore variation of current with time is 'qt'. This finally results into an asymmetric peak shape. At point C, the potential sweep is reversed that leads to continuous decay of current with rate 'qt' until the potential reaches the redox potential. At this potential, overall reduction of O to R takes place causing a cathodic current that ultimately results into a reduction peak (point D).

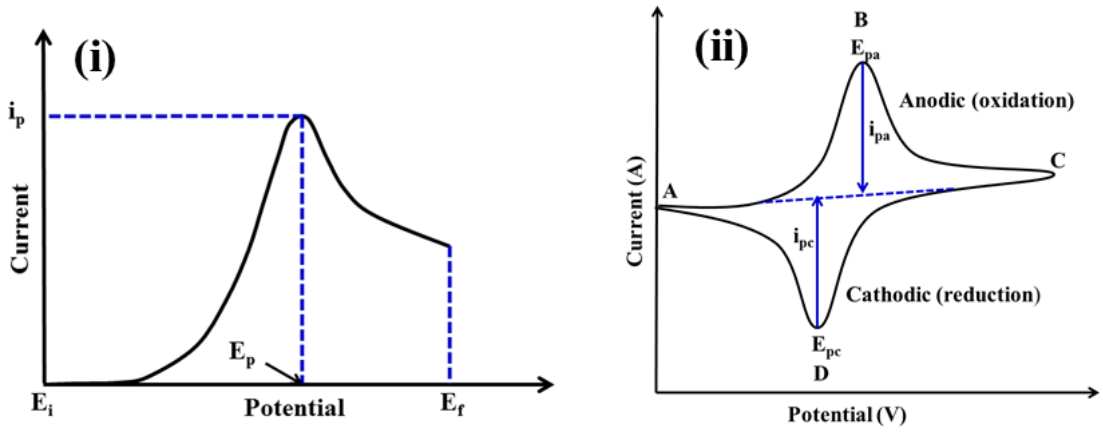

Figure 2.5: *Typical representations of (i) linear sweep voltammetry (LSV) and (ii) cyclic voltammetry (CV) a redox reaction.*

From a cyclic voltammogram, the magnitudes of some important parameters such as anodic peak current (i_{pa}), cathodic peak current (i_{pc}), anodic peak potential (E_{pa}), cathodic peak potential (E_{pc}) and peak to peak separation between anodic and cathodic peaks i.e. ΔE_p (E_{pa}-E_{pc}) can be determined [6]. These parameters are very useful to understand electron transfer process at the electrode and electrolyte interface during an electrochemical reaction as discussed below:

(i) Reversible process

For a reversible process, CV exhibits anodic and cathodic peak potentials with nearby distance and the formal potential (E_f^0) is at or close to the halfway between anodic and cathodic peak potentials (Figure 2.6 (i)). Electron transfer doesn't depend on rate in an electrochemically reversible process and it is rapid enough in comparison to mass transport so that equilibrium is maintained between the reduced and oxidized species of redox couple at the electrode surface.

The diagnostic information for the reversible process [16]:

(a) $\left|\frac{I_{pa}}{I_{pc}}\right| = 1$ (For all scan rates)

(b) $\Delta E_p = \left|E_{pa} - E_{pc}\right| = \frac{59}{n}\text{mV}$ (For all scan rates)

Where n is the number of electrons transferred during redox process.

(c) $I_p \propto \nu^{\frac{1}{2}}$ (ν = scan rate)

(d) E_p is independent of scan rate.

(ii) Quasi-reversible process

For a quasi-reversible process, CV exhibits (Figure 2.6 (ii)) anodic and cathodic peak potentials with a wide separation, and E_f^0 is not close to the halfway between anodic and cathodic peak potentials. In case of a quasi-reversible electron transfer process, the rates of charge transfer and mass transport are almost similar. It is an intermediate between reversible and irreversible processes, since the current is governed by both charge and mass transfer kinetics [14]. This process occurs when the electron transfer rate is not rapid enough as compared to that of mass transport to establish equilibrium between the oxidized and reduced species of redox couple at the surface of electrode.

For a quasi-reversible system, the diagnostic information is given below [8, 16]:

(a) $\left|\frac{I_{pa}}{I_{pc}}\right| = 1$ Provided $\alpha_a = \alpha_c = 0.5$.

(b) $\Delta E_p = \left|E_{pa} - E_{pc}\right| > \frac{59}{n}mV$ and increases with scan rate.

(c) I_p increases with $\nu^{\frac{1}{2}}$ but not proportional to it.

(d) E_{pc} shifts negatively with increasing scan rate.

(iii) Irreversible process

In case of irreversible process, E_f^0 is same, however a large overpotential is necessary to induce electron transfer resulting into a broad anodic peak towards the more positive potential (Figure 2.6 (iii)). This is due to slow charge transfer as compared to mass transfer resulting into a non-equilibrium condition at the electrode surface.

For irreversible process, the diagnostic information is [16]:

(a) No reverse peak is observed.

(b) $\Delta E_p = \left|E_p - E_{\frac{p}{2}}\right| = \frac{47}{\alpha n}\,mV$, Where α is the charge transfer coefficient.

(c) Negative shift of E_p by $\frac{30}{\alpha n}$ mV, for per decade increase in scan rate.

(d) $I_p \propto \nu^{\frac{1}{2}}$

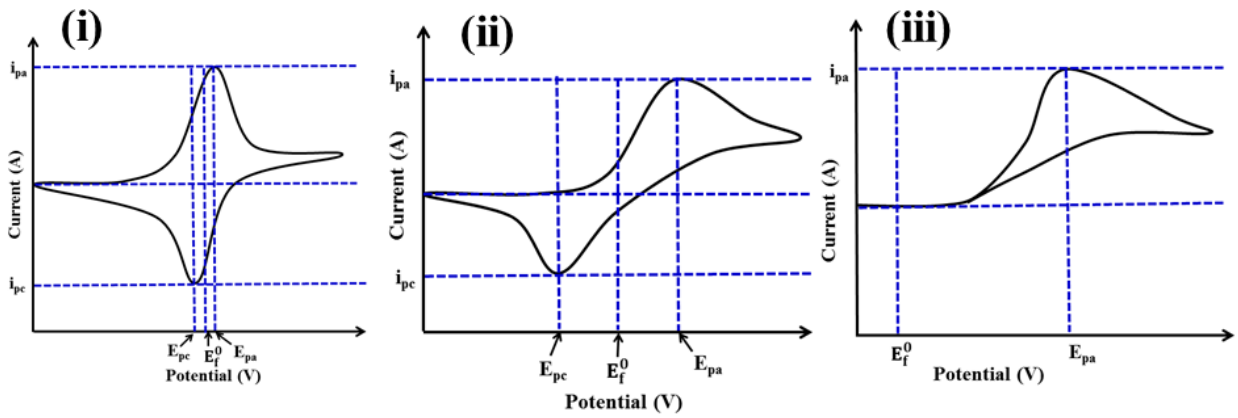

Figure 2.6: *CVs of (i) reversible, (ii) quasi-reversible and (iii) irreversible processes.*

2.2.1 Surface coverage of adsorbed redox active species

The coverage of adsorbed species over the surface of electrode can be determined from CV measurements [17, 18]. The surface coverage is defined as the concentration of redox active species in mol adsorbed over per unit area of the electrode surface. Considering an electrochemical reaction within a potential range, so that the surface coverage (Γ^*) does not depend on applied potential E [18].

Under this condition

$$-\frac{\partial \Gamma_O(t)}{\partial t} = \frac{\partial \Gamma_R(t)}{\partial t} = \frac{i}{nFA} \qquad (2.5)$$

Where Γ_O (t) and Γ_R (t) (mol cm^{-2}) are the surface coverage of oxidized and reduced species at time t and it is written as:

$$\Gamma_O(t) = \frac{\beta_O \Gamma_{O,s} C_O(0,t)}{1+\beta_O C_O(0,t)+ \beta_R C_R(0,t)} \quad (2.6)$$

$$\Gamma_R(t) = \frac{\beta_R \Gamma_{R,s} C_R(0,t)}{1+\beta_O C_O(0,t)+ \beta_R C_R(0,t)} \quad (2.7)$$

Applying the initial conditions, at t=0

$$\Gamma_O = \Gamma_O^* \quad \text{and} \quad \Gamma_R = 0 \quad (2.8)$$

The total surface coverage of adsorbed redox active species is given by using the equations (2.5) and (2.8)

$$\Gamma_O^* = \Gamma_O(t) + \Gamma_R(t) \quad (2.9)$$

Using equations (2.6) and (2.7)

$$\frac{\Gamma_o(t)}{\Gamma_R(t)} = \frac{b_o C_o(0,t)}{b_R C_R(0,t)} \quad (2.10)$$

Where $b_O = \beta_O \Gamma_{O,s}$ and $b_R = \beta_R \Gamma_{R,s}$

If the reaction is Nernstian, so that

$$\frac{C_O(0,t)}{C_R(0,t)} = \exp\left[\left(\frac{nF}{RT}\right)\left(E - E_f^0\right)\right] \quad (2.11)$$

Therefore equation (2.10) can be re-written as

$$\frac{\Gamma_O(t)}{\Gamma_R(t)} = \frac{b_O}{b_R}\exp\left[\left(\frac{nF}{RT}\right)\left(E - E_f^0\right)\right] \quad (2.12)$$

The relation between i and ν can be obtained using the equations (2.5), (2.9) and (2.12)

$$\frac{i}{nFA} = -\frac{\partial \Gamma_O(t)}{\partial t} = \left[\frac{\partial \Gamma_O(t)}{\partial E}\right]\nu \quad (2.13)$$

With $E = E_i - \nu t$, the equation for i-E curve is given by [30]:

$$i = \frac{n^2F^2\nu A\Gamma_O^*(b_O/b_R)\exp[(nF/RT)(E-E_f^0)]}{RT\{1+(b_O/b_R)\exp[(nF/RT)(E-E_f^0)]\}^2} \quad (2.14)$$

The above equation can be expressed as

$$\text{Peak current, } i_p = \frac{n^2F^2\nu A\Gamma_O^*}{4RT} \quad (2.15)$$

Therefore, the value of surface coverage (Γ_O^*) can be obtained from the linear slope of i_p vs. ν.

2.2.2 Laviron's Theory

In Electrochemistry, the rate of charge transfer reactions at the interface between electrode and electrolyte solution is studied using Laviron's theory. In 1979, mathematical formulations were published by Laviron to determine the heterogeneous charge transfer rate constant, k_s and the charge transfer coefficient, α of a redox couple

[19]. It can be calculated from voltammetry measurements by using the change in anodic and cathodic peak potentials as a function of logarithm of scan rate.

Considering a heterogeneous redox reaction as presented below;

$$O + ne \rightleftharpoons R \tag{2.16}$$

The applied potential E can be written as

$$E = E_i + \nu t \tag{2.17}$$

Where E_i initial potential applied in Volt (V) and ν is the scan rate in V s^{-1}.

When O and R species strongly get adsorbed over the electrode surface then the surface standard potential E'^0 is given by [20, 21]

$$E'^0 = E^0 - \frac{RT}{nF}\ln\frac{b_O}{b_R} \tag{2.18}$$

Where b_O and b_R are the adsorption coefficients of O and R species.

We can write the equation for current as given below:

$$i = nFAk_s\left\{\Gamma_O exp\left[-\alpha nF\frac{(E-E'^0)}{RT}\right] - \Gamma_R exp\left[(1-\alpha)nF\frac{(E-E'^0)}{RT}\right]\right\} \tag{2.19}$$

$$\Gamma_O + \Gamma_R = \Gamma_T \tag{2.20}$$

$$i = -nFA\frac{d\Gamma_O}{dt} \tag{2.21}$$

Where k_s is the rate constant, Γ_O and Γ_R are the surface coverage of O and R species in mol cm^{-2}, Γ_T is their constant sum, A is the surface area in cm^2, α is the charge transfer coefficient, i is the current in amperes and n, F, R and T have their usual meanings.

Further Ψ, a dimensionless function has been considered to define current [22]:

$$\Psi = \frac{i}{\left(\frac{F^2}{RT}\right)n^2\nu A\Gamma_T} = m\left[\left(\frac{\Gamma_O}{\Gamma_T}\right)\eta^{-\alpha} - \left(\frac{\Gamma_R}{\Gamma_T}\right)\eta^{1-\alpha}\right] \tag{2.22}$$

$$\text{Where } m = \left(\frac{RT}{F}\right)\left(\frac{k_s}{\eta\nu}\right) \text{ and } \eta = exp\left[\left(\frac{nF}{RT}\right)(E - E'^o)\right] \tag{2.23}$$

Substituting, Γ_O, Γ_R and Γ_T by χ_O, χ_R and χ_T. Then from equations (2.17) and (2.19)-(2.21), a couple of differential equations have been derived as shown below:

$$\frac{d\left(\frac{\chi_O}{\chi_T}\right)}{d\eta} + m(1+\eta)\eta^{-(1+\alpha)}\left(\frac{\chi_O}{\chi_T}\right) = m\eta^{-\alpha} \tag{2.24}$$

$$\frac{d\left(\frac{\chi_R}{\chi_T}\right)}{d\eta} + m(1+\eta)\eta^{-(1+\alpha)}\left(\frac{\chi_R}{\chi_T}\right) = m\eta^{-(1+\alpha)} \tag{2.25}$$

The values of either $\frac{\chi_O}{\chi_T}$ or $\frac{\chi_R}{\chi_T}$ can be determined by solving one of the above equations (2.24) or (2.25) and then it is introduced into equation (2.22) to obtain the expression for Ψ.

For the cathodic curve, Ψ_C can be written as:

$$\Psi_c = m\eta^{-\alpha}\{1 - m(1+\eta)\exp[f(\eta)]\int_{\infty}^{\eta} z^{-(1+\alpha)}\exp[-f(z)]dz\} \quad (2.26)$$

For the anodic curve, Ψ_a can be written as:

$$\Psi_a = -m\eta^{-\alpha}\{\eta - m(1+\eta)\exp[f(\eta)]\int_{0}^{\eta} z^{-\alpha}\exp[-f(z)]dz\} \quad (2.27)$$

$$\text{Where } f(\eta) = \left[\frac{m}{\alpha(1-\alpha)}\right]\eta^{-\alpha}[1-\alpha(1+\eta)] \quad (2.28)$$

m is negative for the cathodic curve and positive for the anodic curve. In limiting form, $m \to 0$ for irreversible or quasi reversible reactions [22], the equations (2.26) and (2.27) yield simplified forms.

Hence considering $m \to 0$,

For the cathodic curve $\eta^{1-\alpha} \ll \eta^{-\alpha}$ and $\eta \ll 1$

The equation (2.26) can be written as

$$\Psi_c = m\eta^{-\alpha}\exp\left(\frac{m\eta^{-\alpha}}{\alpha}\right) \quad (2.29)$$

In similar way, $n^{-\alpha} \ll \eta^{1-\alpha}$ and $\eta \gg 1$ for the anodic curve and equation (2.27) can be expressed as:

$$\Psi_a = -m\eta^{1-\alpha}\exp\left(\frac{-m\eta^{1-\alpha}}{1-\alpha}\right) \quad (2.30)$$

When $\eta^{-\alpha} = \frac{\alpha}{|m|}$, Ψ_c becomes maximum, hence the peak potential, E_p for cathodic reaction is given by

$$\left.\begin{aligned} E_{pc} &= E_f^0 - \frac{RT}{\alpha nF}\ln\left[\frac{\alpha}{|m|}\right] \\ &\text{Or} \\ E_{pc} &= E_f^0 - 2.3RT\frac{\log\nu}{\alpha nF} \end{aligned}\right\} \quad (2.31)$$

When $\eta^{1-\alpha} = \frac{(1-\alpha)}{|m|}$, then the maximum value of Ψ_a is achieved and the E_p for anodic reaction can be written as:

$$\left.\begin{aligned} E_{pa} &= E_f^0 + \frac{RT}{(1-\alpha)nF}\ln\left[\frac{1-\alpha}{|m|}\right] \\ &\text{Or} \\ E_{pa} &= E_f^0 + 2.3RT\frac{\log\nu}{(1-\alpha)nF} \end{aligned}\right\} \quad (2.32)$$

When $m \to \infty$, the reaction tends towards reversible, and both the cathodic and anodic peaks are symmetrical with respect to the potential axis [19, 23, 24]. In this case, the peak potential, E_p does not depend on scan rate.

2.2.2.1 Calculation of heterogeneous rate constant (k_s) and charge transfer coefficient (α)

According to Laviron's theory [19], in quasi-reversible and irreversible systems, the change in both anodic and cathodic peak potentials (E_{pa} and E_{pc}) with scan rate gives two straight lines having slopes equal to $\frac{-2.3\ RT}{nF\alpha_c}$ and $\frac{2.3\ RT}{nF(1-\alpha_a)}$ for the cathodic and anodic peaks, respectively. The heterogeneous rate constant (k_s) can be obtained by inserting the value of α in the following equation:

$$\log k_s = \alpha \log(1-\alpha) + (1-\alpha)\log\alpha - \log\frac{RT}{nF\nu} - \frac{\alpha(1-\alpha)nF\Delta E_P}{2.3\ RT} \qquad (2.33)$$

The higher value of k_s denotes fast re-establishment of equilibrium between O and R species upon application of potential, while the smaller value of k_s indicates slow electron transfer rate causing longer time to reach equilibrium [25]. For different electron transfer processes, the range of k_s is given below [26]:

Reversible process: $k_s > 0.020$ cm s^{-1}

Quasi-reversible process: $0.020 > k_s > 5\times10^{-5}$ cm s^{-1}

Irreversible process: $k_s < 5\times10^{-5}$ cm s^{-1}

The symmetry between forward and backward electron transfer of an electrochemical reaction is measured using charge transfer coefficient (α) [27]. It signifies the fraction of potential at the interface between electrode and electrolyte solution that can lower the energy barrier to occur an electrochemical reaction.

2.3 Butler-Volmer kinetics

The reaction kinetics of faradaic processes that occur at the electrode surface is greatly affected by the electrode potential. Therefore, the electron transfer rate between the surface of electrode and the electroactive species can be changed by varying the potential applied at the electrode [28]. The relation between electron transfer rate and applied potential can be obtained using Butler-Volmer model. Considering an electron transfer reaction between an oxidized (O) and reduced species (R)

$$O + ne \underset{k_b}{\overset{k_f}{\rightleftharpoons}} R \qquad (2.34)$$

Where, k_f and k_b are the heterogeneous rate constants of the reduction and oxidation reactions, respectively and n is the number of electrons exchanged during reaction. The

net current (i) consists of both cathodic (i_c) and anodic (i_a) components that are shown below [8]:

$$i_c = -nFAk_f C_O(0,t) \quad (2.35)$$

$$i_a = nFAk_b C_R(0,t) \quad (2.36)$$

Where $C_O(0,t)$ and $C_R(0,t)$ are the concentrations of O and R forms at the electrode surface at any time t and F is the Faraday constant.

The total current at any time t can be written as [8]:

$$i = i_a + i_c = nFA[k_b C_R(0,t) - k_f C_O(0,t)] \quad (2.37)$$

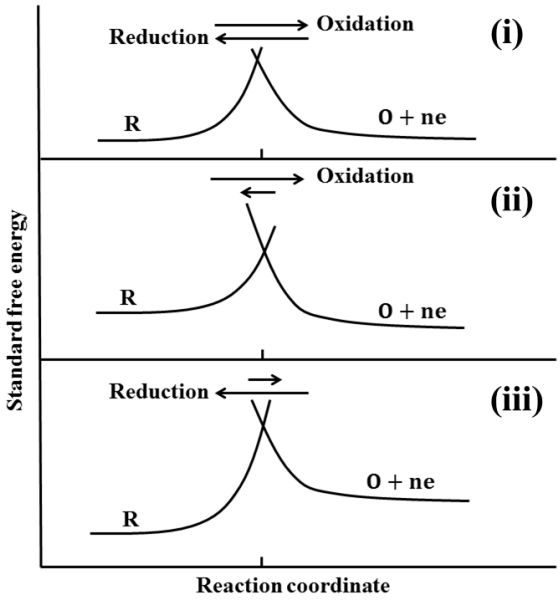

Figure 2.7: *The graphical display of changes in standard free energy during a faradaic process. (i) At a potential that corresponds to the equilibrium. (ii) At a potential more positive than the equilibrium value. (iii) At a potential more negative than the equilibrium value.*

Figure 2.7 shows progress of a reaction along a reaction coordinate. The point of intersection of reactant and product configurations shown in Figure 2.7 is termed as transition state since at this state transfer of electrons occurs between the redox active species. The relative height of the activation energy barriers represents the reaction rate. The system attains equilibrium when both the rates of oxidation and reduction reactions are equal to each other (Figure 2.7 (i)) and the corresponding potential is E_{eq} [29]. The energy of the reactant electron decreases as the potential goes towards more positive value (Figure 2.7 (ii)). Hence, there is a drop of the energy curve that corresponds to O

and oxidation occurs. In contrast, when the potential is lower (Figure 2.7 (iii)) than the equilibrium value, then height of the activation energy barrier for oxidation increases and therefore reduction reaction takes place.

The effect of potential on the electron transfer rate can be given by the following equations [8, 28]:

$$k_f = k_f^0 \exp\left[-(1-\alpha)\frac{nFE}{RT}\right] \quad (2.38)$$

$$k_b = k_b^0 \exp\left[\alpha\frac{nFE}{RT}\right] \quad (2.39)$$

Where E is the applied potential, α is the transfer coefficient and its value lies in between 0 to 1 and k_f^0 and k_b^0 are the rate constants at E=0.

From the equations (2.37), (2.38) and (2.39), we can write:

$$i = nFA\left[k_b^0 C_R(0,t)\exp\left(\alpha\frac{nFE}{RT}\right) - k_f^0 C_O(0,t)\exp\left(-(1-\alpha)\frac{nFE}{RT}\right)\right] \quad (2.40)$$

At formal potential (E_f^0), bulk concentrations of both oxidized and the reduced species are equal i.e. $C_O^* = C_R^*$. In this situation $k_f C_O^* = k_b C_R^*$ such that $k_f = k_b$. Thus, at the potential E_f^0, the value of reduction and oxidation rate is same and it can be defined as standard rate constant, k^0. The rate constants in equations (2.38) and (2.39) can be expressed in terms of k^0 and the difference between E and E_f^0.

$$k_f = k^0 \exp\left[-(1-\alpha)\frac{nF\,(E-E_f^0)}{RT}\right] \quad (2.41)$$

$$k_b = k^0 \exp\left[\alpha\frac{nF(E-E_f^0)}{RT}\right] \quad (2.42)$$

k^0 can be physically interpreted as a measure of kinetic facility of a redox active species. A large k^0 value (within the range of 1 to 10 cm s^{-1}) indicates fast reaction that can attain equilibrium within a very short period of time while a small k^0 value (can be smaller than 10^{-9} cm s^{-1}) implies a sluggish reaction kinetics [30].

By inserting the equations (2.41) and (2.42) into equation (2.40), we obtain:

$$i = nFAk^0\left[C_R(0,t)\exp\left(\alpha\frac{nF(E-E_f^0)}{RT}\right) - C_O(0,t)\exp\left(-(1-\alpha)\frac{nF(E-E_f^0)}{RT}\right)\right] \quad (2.43)$$

At equilibrium potential (E_{eq}), the net current is zero and the equation (2.43) can be written as

$$nFAk^0 C_R(0,t)\exp\left[\alpha\frac{nF(E_{eq}-E_f^0)}{RT}\right] = nFAk^0 C_O(0,t)\exp\left[-(1-\alpha)\frac{nF(E_{eq}-E_f^0)}{RT}\right] \quad (2.44)$$

At equilibrium condition, the bulk concentration of O and R form is equal to its concentration at the electrode surface, thus

$$\exp\left[\frac{nF}{RT}\left(E_{eq}-E_f^0\right)\right] = \frac{C_O^*}{C_R^*} \quad (2.45)$$

Hence, from equation (2.45) the Nernst equation can be written as:

$$E_{eq} = E_f^0 + \frac{RT}{nF} \ln \frac{C_O^*}{C_R^*} \tag{2.46}$$

In E_{eq}, an important parameter known as exchange current density (i_0) is introduced to define the rate of electron exchange between the electrode surface and the redox active species in the solution. However, the rates of electron exchange in both the directions of interface are equal and opposite and therefore the overall electron exchange is zero in equilibrium condition. The magnitude of i_0 is equal to i_c or i_a and can be expressed as [31]:

$$i_0 = nFAk^0 C_O^* \exp\left[-(1-\alpha)\frac{nF(E_{eq}-E_f^0)}{RT}\right] \tag{2.47}$$

Both sides of the equation (2.45) are raised to the $-(1-\alpha)$ power and can be re-written as:

$$\exp\left[-(1-\alpha)\frac{nF(E_{eq}-E_f^0)}{RT}\right] = \left(\frac{C_O^*}{C_R^*}\right)^{-(1-\alpha)} \tag{2.48}$$

Substituting equation (2.48) into (2.47), we obtain

$$i_0 = nFAk^0 {C_O^*}^{\alpha} {C_R^*}^{(1-\alpha)} \tag{2.49}$$

In equilibrium condition $C_O^* = C_R^* = C$

Then equation (2.49) is given by the following expression:

$$i_0 = nFAk^0 C \tag{2.50}$$

Now, dividing equation (2.43) by (2.49), the following expression is obtained:

$$\frac{i}{i_0} = \frac{C_R(0,t)\exp\left(\alpha\frac{nF(E-E_f^0)}{RT}\right)}{{C_O^*}^{\alpha}{C_R^*}^{(1-\alpha)}} - \frac{C_O(0,t)\exp\left(-(1-\alpha)\frac{nF(E-E_f^0)}{RT}\right)}{{C_O^*}^{\alpha}{C_R^*}^{(1-\alpha)}} \tag{2.51}$$

$$\frac{i}{i_0} = \frac{C_R(0,t)}{C_R^*}\exp\left(\alpha\frac{nF(E-E_f^0)}{RT}\right)\left(\frac{C_R^*}{C_O^*}\right)^{\alpha} - \frac{C_O(0,t)}{C_O^*}\exp\left(-(1-\alpha)\frac{nF(E-E_f^0)}{RT}\right)\left(\frac{C_R^*}{C_O^*}\right)^{-(1-\alpha)} \tag{2.52}$$

From the equations (2.45) and (2.48), the ratios $\left(\frac{C_R^*}{C_O^*}\right)^{\alpha}$ and $\left(\frac{C_R^*}{C_O^*}\right)^{-(1-\alpha)}$ are evaluated and substituted in equation (2.52) and obtained as [32]:

$$i = i_0\left[\frac{C_R(0,t)}{C_R^*}\exp\left(\alpha\frac{nF}{RT}\eta\right) - \frac{C_O(0,t)}{C_O^*}\exp\left(-(1-\alpha)\frac{nF}{RT}\eta\right)\right] \tag{2.53}$$

Where, $\eta = E - E_{eq}$ is the extent of deviation of applied potential from the equilibrium potential and it is termed as overpotential. In equation (2.53), the first term denotes contribution from the anodic part of current while the second term comes from the cathodic contribution of current.

If the solution is well stirred or the current is kept sufficiently low then the concentrations of oxidant and reductant at the electrode surface are almost same to the bulk value. Hence, the equation (2.53) becomes [8]:

$$i = i_0 \left[\exp\left(\alpha \frac{nF}{RT}\eta\right) - \exp\left(-(1-\alpha)\frac{nF}{RT}\eta\right)\right] \quad (2.54)$$

The above equation is known as Butler-Volmer equation. Figure 2.8 depicts the relation between current and overpotential as described in equation (2.54).

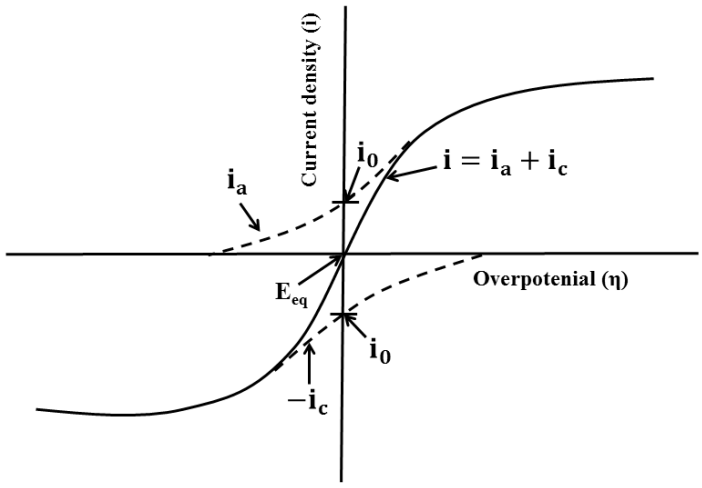

Figure 2.8: *A plot of current against the overpotential according to Butler-Volmer equation.*

2.3.1 Tafel analysis

Butler-Volmer equation discusses an exponential relationship between current density (i), overpotential (η) and exchange current density (i_0) without mass transfer effect. A small amount of overpotential is needed to drive a reaction if the value of i_0 is high and the system is reversible [32]. In such systems current can flow in both the anodic and cathodic directions contributing towards the net current. However, a large amount of overpotential is required to drive a reaction if i_0 is small and the system is irreversible [30]. In such systems the electron transfer rate is slow; hence a long time is needed by the system to attain equilibrium.

When a large positive overpotential is applied, then anodic process is dominant and cathodic process can be neglected. Hence, the Butler-Volmer equation reduces to following form [8]:

$$\log i = \log i_0 + \frac{\alpha nF}{2.303RT}\eta \quad (2.55)$$

Likewise, if negative overpotential is applied, then cathodic process is favoured and anodic process is negligible. Therefore the equation (2.54) can be written as [8]:

$$\log(-i) = \log(i_0) - \frac{(1-\alpha)nF}{2.303RT}\eta \qquad (2.56)$$

The above expressions (2.55) and (2.56) are termed as Tafel equations. A linear plot of logarithm of the current (log i) vs. overpotential (η) is known as Tafel plot (Figure 2.9).

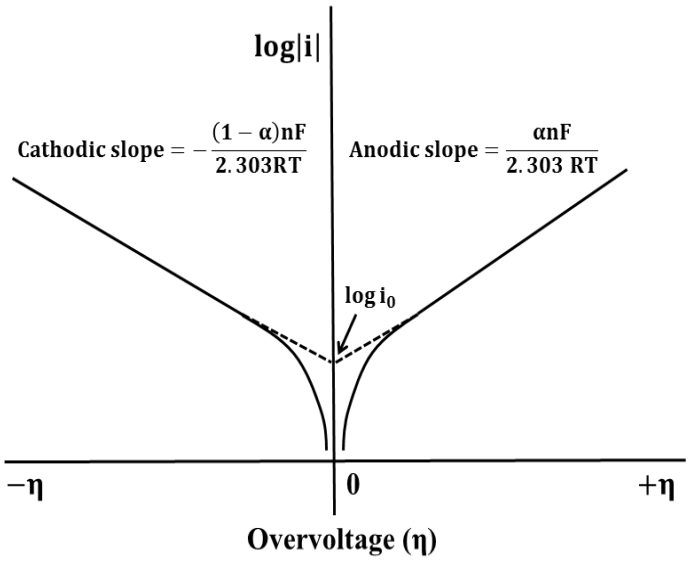

Figure 2.9: *Tafel plot for anodic and cathodic parts of the current-overpotential curve.*

From the equations (2.55) and (2.56), anodic Tafel slope given by $\frac{\alpha nF}{2.303RT}$ and cathodic Tafel slope given by $-\frac{(1-\alpha)nF}{2.303RT}$ can be calculated. Tafel slope is an important parameter to understand the electrocatalytic performance of a catalyst. Larger values of Tafel slope suggest fast increase in overpotential with the increase in current and the smaller values of Tafel slope indicate slow increase in overpotential at high current [32]. From the slope of a Tafel plot, the transfer coefficient (α) can be calculated while the intercept of the line gives the value of exchange current density (i_0).

2.4 Electrochemical Impedance Spectroscopy (EIS)

Electrochemical impedance spectroscopy (EIS) is a powerful tool to investigate different kinds of chemical, electrochemical and surface processes taking place at the interface between the electrode and electrolyte. In EIS technique, the electrode potential is perturbed from the equilibrium potential by applying a small sinusoidal potential (within

the amplitude range of 2-10 mV) in an electrochemical cell over a broad range of frequencies (from 10^{-4} to 10^{8} Hz) [33] . The response of this perturbation is a sinusoidal current signal at the same frequency but differs in phase angle from the applied potential.

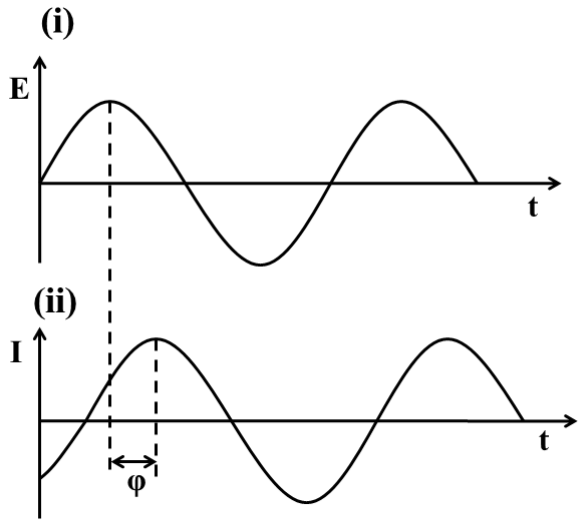

Figure 2.10: *(i) The input sinusoidal potential and (ii) corresponding current signal in output of the electrochemical cell.*

Figure 2.10 represents the input sinusoidal potential and the response current signal of electrochemical cell. The difference in phase of the response signal in relative to the input signal over a wide range of frequencies are very useful to investigate the various electrode processes such as formation and charging of the electric double layer, charge transfer kinetics in ionic or electronic or mixed conductors, diffusion of redox species and homogeneous and heterogeneous electron transfer kinetics [6].

Impedance is defined as the obstruction offered by an electrical system to the flow of charge carriers and can be expressed in terms of unit Ohms, Ω. If the phase difference between the resulting electric current and input potential is zero, then it is termed as resistance, which is independent of frequency. Hence, Ohm's law is applicable under these conditions:

$$E = IR \tag{2.57}$$

Where, E is the input potential in Volt (V), I is the current in ampere (A) and R is the resistance.

When a sinusoidal potential is applied to an electrochemical cell which is a combination of resistors, capacitors or inductors, then there will be a phase difference in the resulting current that flows through the circuit with respect to the applied potential. Thus, the alternating potential, E(t) and current I(t) can be expressed as [34]:

$$E(t) = E_0 \sin(\omega t) \tag{2.58}$$

$$I(t) = I_0 \sin(\omega t + \varphi) \tag{2.59}$$

Where, E_0 and I_0 are the amplitudes of potential and current, respectively, ω is the angular frequency and can be defined as $\omega = 2\pi f$, f is the frequency, φ is the phase shift of measured current signal with respect to the applied potential and t is the time.

The Electrochemical Impedance (Z) can be defined as the ratio between input potential and resulting current and can be expressed in terms of the magnitude (Z_0) and phase difference (φ):

$$Z(\omega) = \frac{E(t)}{I(t)} = \frac{E_0 \sin(\omega t)}{I_0 \sin(\omega t+\varphi)} = Z_0 \frac{\sin(\omega t)}{\sin(\omega t+\varphi)} \tag{2.60}$$

Considering E(t) and I(t) are in complex plane, then these can be expressed as:

$$E(t) = E_0 \exp(j\omega t) \tag{2.61}$$

$$I(t) = I_0 \exp[j(\omega t + \varphi)] \tag{2.62}$$

Where j is the imaginary number and $j = \sqrt{-1}$.

Using Euler's relation, $\exp(j\theta) = \cos\theta + j\sin\theta$, the impedance, Z can be represented in complex form:

$$Z(\omega) = \frac{E_0 \exp(j\omega t)}{I_0 \exp[j(\omega t + \varphi)]} = Z_0 \exp(-j\varphi) = Z_0(\cos\varphi - j\sin\varphi)$$

$$= Z' + j(-Z'') \tag{2.63}$$

The magnitude of Z is given by:

$$|Z(\omega)| = \sqrt{(Z')^2 + (-Z'')^2} \tag{2.64}$$

and the phase angle can be expressed as:

$$\varphi = \tan^{-1}\left(\frac{Z''}{Z'}\right) \tag{2.65}$$

The total impedance, $Z(\omega)$ can be expressed as the sum of a real (Z') and an imaginary (Z'') components. The real component of impedance is resistance and the imaginary component is reactance that appears due to 90^o phase difference between the current and voltage [35]. Based on the sign of phase difference between the current and voltage, the reactance can be divided into inductive reactance (X_L) and capacitive reactance (X_C). In case of inductors, $X_L = \omega L$, where L is the inductance, while X_C of capacitive element is negative and can be written as $X_C = -\frac{1}{\omega C}$, where C is the capacitance. The resulting impedance spectra obtained by plotting Z' on the X-axis and Z'' on the Y-axis are known as Nyquist plot and shown in Figure 2.11(i).

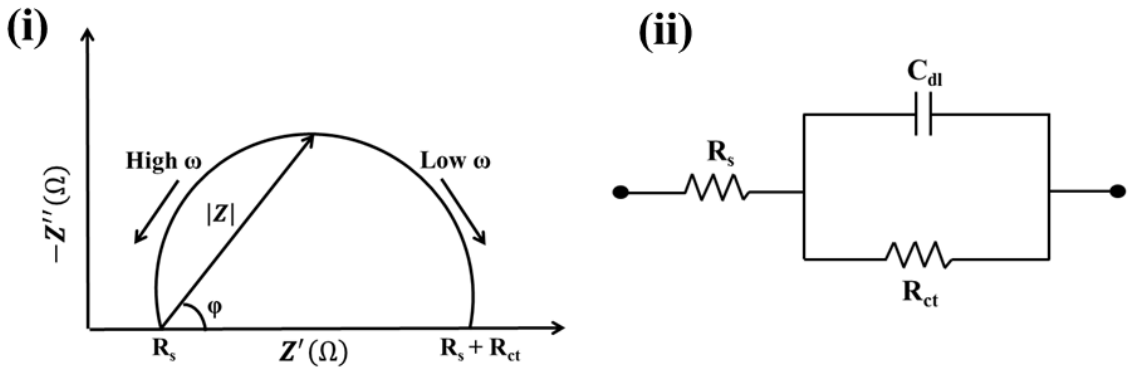

Figure 2.11: *(i) Nyquist plot and (ii) corresponding simplified Randles equivalent circuit.*

In Nyquist plot, Y-axis is negative and every point on this plot signifies the impedance at a certain frequency [36]. The magnitude of the impedance can be represented by a vector of length |Z| and the anticlockwise angle between this vector and X-axis is given by phase angle, φ. The Nyquist plot is used to analyse the electrochemical processes taking place within the system and can be interpreted as equivalent electrical circuit model consisting of resistors, inductors and capacitors. The parameters such as solution resistance (R_s), charge transfer resistance (R_{ct}) and double layer capacitance (C_{dl}) can be obtained by proper fitting of the experimental data to the electrical circuit model [37]. The simplified Randles equivalent circuit in Figure 2.11 (ii) is the most common circuit model and used to fit the Nyquist plot depicted in Figure 2.11 (i).

The impedance in Randles equivalent circuit can be written as [38, 39]:

$$Z(\omega) = R_s + \frac{R_{ct}}{1+\omega^2 R_{ct}^2 C_{dl}^2} - j\frac{\omega R_{ct}^2 C_{dl}}{1+\omega^2 R_{ct}^2 C_{dl}^2} \tag{2.66}$$

The real and imaginary components of impedance can be written from equation (2.66) as:

$$Z'(\omega) = R_s + \frac{R_{ct}}{1+\omega^2 R_{ct}^2 C_{dl}^2} \tag{2.67}$$

$$Z''(\omega) = -\frac{\omega R_{ct}^2 C_{dl}}{1+\omega^2 R_{ct}^2 C_{dl}^2} \tag{2.68}$$

At high frequencies such as $\omega \to \infty$, the terms that dependent on frequency in equation (2.67) vanish and $Z(\omega) = R_s$. Hence, the impedance is resistive and phase angle is zero at high frequencies and it is given by the intercept on real axis. However, at low frequencies, such as $\omega \to 0$, $Z(\omega) = R_s + R_{ct}$ and it is given by the intercept on real axis at low frequency side of the Nyquist plot.

Considering that ω_{max} is the frequency at which $-Z''(\omega)$ becomes maximum. Hence, for the maximum $-Z''(\omega)$, it is written as [40]:

$$\omega_{max} R_{ct} C_{dl} = 1 \tag{2.69}$$

Therefore C_{dl} can be written as [40]:

$$C_{dl} = \frac{1}{\omega_{max} R_{ct}} \tag{2.70}$$

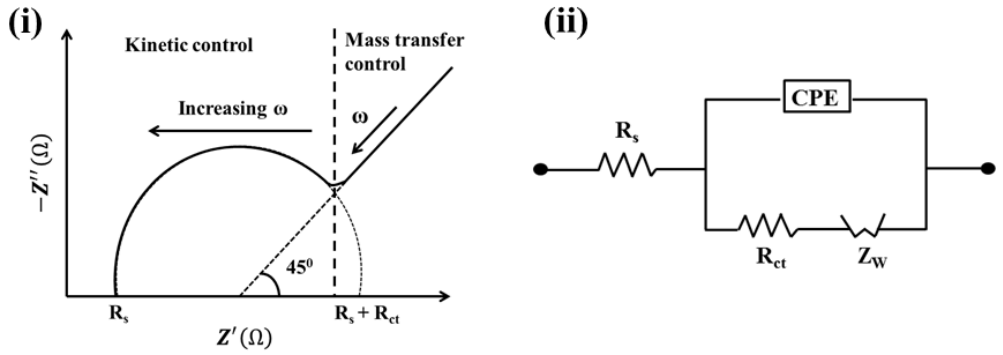

Figure 2.12: *(i) Nyquist plot for a mixed circuit and (ii) corresponding Randles equivalent circuit.*

The non-ideal behaviour of C_{dl} is mainly due to inhomogeneous electrode surface resulting from surface roughness, presence of impurities and grain boundaries [8]. Hence, the pure capacitor is replaced by a constant phase element (CPE). Moreover, another circuit element Warburg diffusion element is introduced when the charge transfer kinetics is influenced by diffusion process in an electrochemical system and it is in series combination with R_{ct} [36]. The Warburg element gives rise to a straight line with a slope of 45^o at a lower frequency side of the Nyquist plot as shown in Figure 2.12 (i). The complete Randles equivalent circuit with CPE and Warburg impedance element is depicted in Figure 2.12 (ii).

2.4.1 Different impedance parameters in an electrochemical cell system

A brief discussion of different types of impedances offered by the elements of an electrochemical system such as resistor and capacitor to the flow of charges is given below:

(i) Solution resistance (R_s)

Current flows through an electrical circuit upon application of a voltage at the electrode of an electrochemical system. The amount of current flow is dependent on the

concentration of electrolyte solution. The electrons can flow from the anode to cathode through an electrolytic solution, where ions in the solution act as electron carrier [36]. Presence of more number of ions in the solution decreases the resistance. Moreover, ionic resistance not only depends on the concentration of solution but also it is influenced by type of ions, temperature and geometry of the area containing the electrolyte solution [38]. The resistance of solution can be expressed as:

$$R = \rho \frac{l}{A} \tag{2.71}$$

Where, ρ is the solution resistivity, l is the length and A is the area of the cell containing solution.

(ii) Double layer capacitance (C_{dl}) and constant phase element (CPE)

The formation of an electrical double layer at the electrode-electrolyte interface is due to adsorption of ions from the electrolyte solution and accumulation and rearrangement over the electrode surface. Electric double layer prevents the flow of current and thus acts as a capacitor. The value of double layer capacitance (C_{dl}) is governed by various factors such as concentration of ions, electrode potential, types of ions, temperature, roughness and high porosity of the electrode surface, adsorption of impurity ions etc. [41]. Therefore, electrode-electrolyte interface can't be considered as ideal capacitor and constant phase element (CPE) is used to replace conventional capacitor. The impedance associated with CPE is given by [42]:

$$Z_{CPE} = \frac{1}{C_0(j\omega)^n} \tag{2.72}$$

Where, C_0 is the capacitance and n is the exponent, $-1 \leq n \leq 1$. Based on the value on n, Z_{CPE} changes and it has different physical significances. When $n = 0$ the CPE corresponds to a pure resistor and when n approaches to 1, the CPE resembles a capacitor and it becomes a perfect capacitor with capacitance C_0 when $n = 1$. CPE represents a pure inductor when $n = -1$ and it corresponds to an infinite Warburg impedance when $n = 0.5$ [42].

(iii) Charge transfer resistance (R_{ct})

The charge transfer resistance (R_{ct}) is the opposition to transfer of charges at the electrode-electrolyte interface and therefore it is associated to reaction kinetics. Hence, the flow of current in electrode is influenced by the value of R_{ct}. In an electrochemical reaction given by equation (2.34), the electrons enter into the electrode and the charge transfer occurs from the electrode to electrolyte solution [33]. The speed of charge

transfer reaction is governed by the reaction type, concentration of products obtained from the reaction, potential and temperature. Butler-Volmer equation as shown in equation (2.54) is applicable when the polarization is dependent on charge transfer kinetics. Assuming η is very small and the electrochemical system is at equilibrium, then R_{ct} can be written as [43, 44]:

$$R_{ct} = \frac{RT}{nFi_0} \tag{2.73}$$

Where i_0 is the exchange current density and the other terms have usual meanings.

(iv) Warburg Impedance (Z_W)

Diffusion of reactants from the bulk solution to the electrode surface plays a significant role in mass transport phenomenon. It results into a frequency dependent impedance parameter known as Warburg impedance (Z_W) [8]. At low frequencies, the value of Z_W is high since the reactants have to move a long distance to reach the electrode surface while; it is negligible at high frequencies as the reactants do not have to travel very far. For a bounded system i.e. finite diffusion, the impedance can be expressed as given below [44]:

$$Z_O = \sigma\omega^{-\frac{1}{2}}(1 - j)\tanh\left[\delta\left(\frac{j\omega}{D}\right)^{\frac{1}{2}}\right] \tag{2.74}$$

Where σ is the Warburg coefficient and can be written as [44]:

$$\sigma = \frac{RT}{n^2F^2A\sqrt{2}}\left[\frac{1}{C_O^*\sqrt{D_O}} + \frac{1}{C_R^*\sqrt{D_R}}\right] \tag{2.75}$$

ω is the angular frequency, δ is the thickness of Nernst diffusion layer, D is the average of diffusion coefficients of diffusing species, A is the electrode surface area, n is the number of electrons transferred and D_O and D_R are the diffusion coefficients of the oxidant and reductant, respectively.

When the thickness of diffusion layer is infinite, then equation (2.74) is simplified and expression for Warburg impedance is obtained as shown below [44]:

$$Z_W = \sigma\omega^{-\frac{1}{2}} - j\sigma\omega^{-\frac{1}{2}} \tag{2.76}$$

2.5 Chronoamperometry (CA)

Chronoamperometry is a quantitative analysis technique to observe steady state polarization during electrooxidation process. In this case, the current response is recorded against a constant electrode potential over a period of time. The detail information regarding the oxidation mechanisms and kinetics of the system can be obtained with the help of this technique [6]. In addition, poisoning rate of the electrode along with

adsorption isotherm can also be determined by this method. In this method, the potential of working electrode at E_1 (in general, no faradaic reaction occurs at this potential) jumps to E_2, at which the faradaic reaction corresponding to mass transfer limited process occurs and surface concentration at the electrode becomes zero (Figure 2.13 (i)). Initially, large current flows and then it decays with time as a result of depletion of the electroactive species over the surface of electrode [45]. The continuous growth of diffusion layer with increase in time causes depletion of the reactants and thereby decreasing the concentration gradient as time goes on. The corresponding current can be calculated for simple systems: $R \rightarrow O + ne^-$, where initially only O or R species are present [6]. The diffusion limited or faradaic current at a planar electrode is given by Cottrell equation [8]:

$$i_f = \frac{nFACD^{\frac{1}{2}}}{\pi^{\frac{1}{2}} t^{\frac{1}{2}}} = kt^{-\frac{1}{2}} \qquad (2.77)$$

Where, n is the number of electrons involved in redox reaction, F is the Faraday constant (96,485 C mol^{-1}), A is the area of planar electrode in cm^2, C is the bulk concentration in mol cm^{-3}, D is the diffusion coefficient in cm^2 s^{-1} and time t in s.

The resulting plot of current vs. time (i-t) as shown in Figure 2.13 (ii) is known as chronoamperogram.

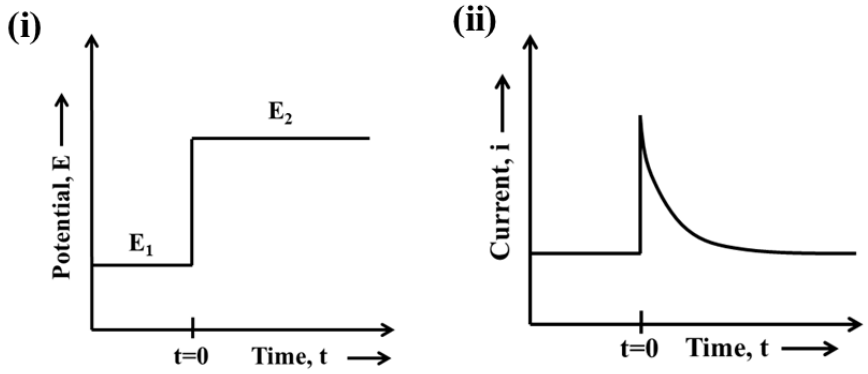

Figure 2.13*: Plots of (i) potential as a function of time and (ii) current as a function of time.*

The i-t graph consisting of two current components: the capacitive current (i_c) due to charging of double-layer, which arises upon changing the potential from E_1 to E_2 and faradaic current (i_f) current due to transfer of electron with the electroactive species as presented in Figure 2.14. From Cottrell equation, it is seen that i_f depends on the area of electrode. The shapes of both i_f and i_c (Figure 2.14) are similar as depicted in Figure 2.13 (ii) indicating that initially at t=0, the current is largest and then they decay over the

period of time; however, there is much faster decay of i_c than that of i_f [40]. The current response over the period of time provides knowledge regarding the reactions responsible for it. i_c ($\propto e^{-\frac{t}{RC}}$, with R = solution resistance and C = capacitance) is dominant at short times while i_f ($\propto t^{-\frac{1}{2}}$) is dominant over a longer period of time. The Cottrell equation can be applied to the systems obeying the following boundary conditions [31]: (a) at t=0, only an electroactive species is present in solution, (b) the solution is considerably large so that the concentration of electroactive species reaches to bulk value at a distance far from the electrode surface, and (c) instantly after the potential step, the concentration of electroactive species is reduced to zero.

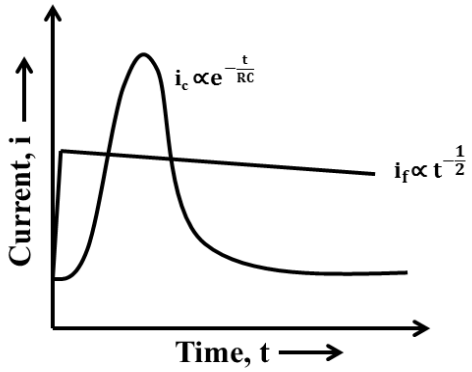

***Figure 2.14**: A plot showing the capacitive current (i_c) and faradaic current (i_f) as a function of time upon application of a potential step.*

2.6 The Brunauer-Emmett-Teller (BET) Theory

The Brunauer-Emmett-Teller (BET) theory deals with physical adsorption of gas molecules on a solid surface and it is employed to determine the specific surface area of a material. A chemically inert gas nitrogen is usually used as adsorbate and the BET experiments are performed at the boiling point of nitrogen i.e. 77 K [46]. Since the process is reversible due to weak van der Waal interaction between adsorbate and adsorbent, hence the experiment is termed as N_2 adsorption-desorption measurements. The BET theory is based on five major assumptions [47]. First is formation of monolayer due to adsorption of one molecule on each distinct adsorption site. Second is that an adsorbed molecule can be treated as an adsorption site for additional molecules to form additional layer. Third assumption is that the approximation of uppermost layer as liquid phase, which will be in equilibrium with the vapour phase. Fourth is the requirement of a quantity of heat for adsorption/desorption process. The desorption energy for each

molecule in the layer at the solid surface is equal and presented as E_1 so that for all additional layers equals $E_2 = E_3 = \ldots = E_n = E_L$, the heat of liquefaction. Fifth assumption is that when p/p_o approaches unity, the number of layer reaches to infinity. Langmuir theory which deals with monolayer molecular adsorption model is used for multilayer adsorption during BET analysis [48]. The plot between volume of adsorbate adsorbed on the surface of adsorbent versus p/p_o value at constant temperature is known as adsorption-desorption isotherm, which explains the adsorption phenomenon. Here, p is the equilibrium vapour pressure and p_o is the saturation vapour pressure of the adsorbates at the temperature of adsorption and the corresponding graph is termed as the BET adsorption isotherm. BET equation can be written as [49]:

$$\frac{1}{v\left[\left(\frac{p_o}{p}\right)-1\right]} = \frac{c-1}{v_m c}\left(\frac{P}{P_o}\right) + \frac{1}{v_m c} \tag{2.78}$$

$$c = \exp\left(\frac{E_1 - E_2}{RT}\right) \tag{2.79}$$

Where $(E_1\text{-}E_2)$ is the net heat absorbed, v and v_m are the total quantity of gas adsorbed and quantity of monolayer adsorbed gas while c is the BET constant.

The plot of $\frac{1}{v\left[\left(\frac{p_o}{p}\right)-1\right]}$ on y-axis versus $\frac{p}{p_o}$ on x-axis gives a straight line, which is called as the BET plot. The linear characteristic is obtained using the equation (2.78) only within the range of $0.05 < \frac{p}{p_o} < 0.35$. The value of v_m and c can be obtained from the slope and intercept of the resulting straight line as shown in the following equation [49]:

$$v_m = \frac{1}{\text{Slope} + \text{Intercept}} \tag{2.80}$$

$$c = 1 + \frac{\text{Slope}}{\text{Intercept}} \tag{2.81}$$

The total surface area, S_{total} and specific surface area S_{BET} can be obtained with help of following equations and using the values of v_m and c.

$$S_{total} = \frac{v_m N_A s}{V} \tag{2.82}$$

Where N_A is Avogadro's number, V is the molar volume of adsorbate gas and s is the adsorption cross section of the adsorbing material [46].

$$S_{BET} = \frac{S_{total}}{m} \tag{2.83}$$

Where, m is the mass of the adsorbent.

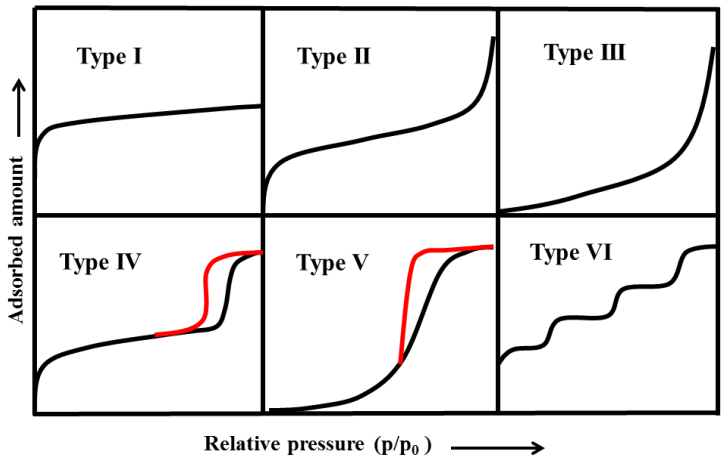

Figure 2.15: *Different types of N_2 adsorption-desorption isotherms according to IUPAC (International Union of Pure and Applied Chemistry).*

According to IUPAC (International Union of Pure and Applied Chemistry), the adsorption-desorption isotherms are classified into six types based on the porosity of different materials as presented in Figure 2.15 [50]. Type I is termed as Langmuir isotherm corresponding to monolayer formation in microporous solids. The curve shows a plateau indicating the maximum adsorption capacity that depends on the volume of available micropore [51]. Type II and III both indicate non-porous or macroporous adsorbents allowing formation of unrestricted monolayer-multilayer at high pressures. Based on the strength of fluid-wall attractive forces, type II and type III can be distinguished. These forces are strong for type II and weak for type III. Since in type I, II and III isotherms no hysteresis loop is observed on reducing the pressure, therefore these are all known as reversible isotherms [52, 53]. Type IV isotherm indicates the presence of mesopores in the material as it exhibits a hysteresis loop due to blockage of pore during desorption of adsorbate. A hysteresis loop is also observed in type V indicating the existence of mesoporous structure. However, the fluid-wall forces are strong in type IV while it is weak in type V. Type VI or stepped isotherm is related to multilayer adsorption on uniform non-porous surfaces [53, 54].

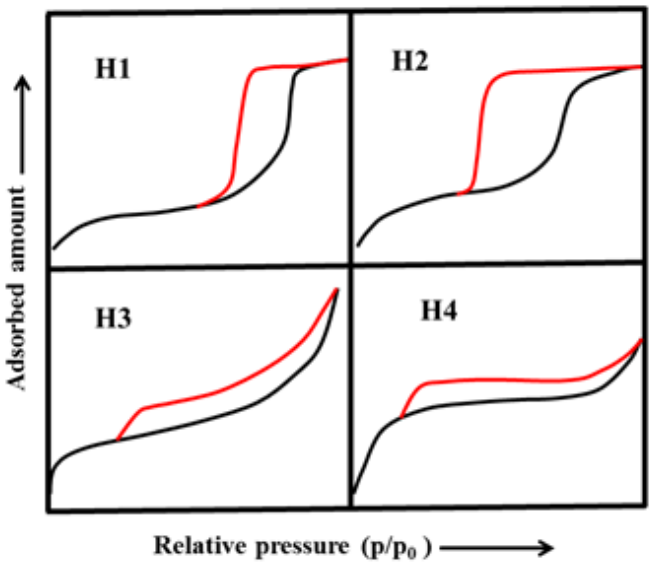

***Figure 2.16**: Different types of hysteresis loop according to IUPAC's classification.*

In 1985, hysteresis loops have been classified by IUPAC into four types based on the width of loop, as shown in Figure 2.16. Temperature, pore structure and the lower closure point influence width of the loop. The closure point depends on the nature of the fluid being adsorbed although it is independent of nature of the porous adsorbent [51]. Both the adsorption and desorption branches are steep at intermediate relative pressures in type H1 indicating the presence of uniform capillary tube like porous structures open at both ends. A broad flat plateau is observed in type H2 with steep desorption branch at intermediate relative pressures corresponding to ink-bottle shaped pore structure. Steep adsorption branch is observed at saturation pressure while at intermediate relative pressures, the desorption branch is steep in type H3 loop. It is associated with open slit-shaped pores. Type H4 loops also suggest the presence of slit-shaped pores and these are seen in materials containing both micropores and mesopores [55].

2.7 The Barrett, Joyner and Halenda (BJH) method

In 1951, the Barret-Joyner-Halenda (BJH) method was developed to understand the capillary condensation phenomenon in a cylindrical pore and also to calculate the pore size distribution (PSD) with the help of Kelvin equation. This method considers that all pores are cylindrical in shape and non-intersecting and carbon's surface has complete wettability, hence Kelvin equation is valid in this case. The Kelvin equation gives relationship between the relative pressure (p/p_o) and the meniscus curvature of liquid

condensed in a pore. The Kelvin equation for cylindrical shaped pore can be expressed as following [56]:

$$\ln \frac{p}{p_o} = \frac{-2\gamma \bar{V}}{r_m RT} \tag{2.84}$$

Where, p is the actual vapour pressure, p_o is the saturation vapour pressure, γ is the surface tension of liquid, $\bar{V}$ is the molar volume of condensed liquid, r_m is the mean radius of curvature of liquid meniscus, R is the universal gas constant and T is the temperature.

The Kelvin radius at which N_2 condensation occurs at a certain relative pressure can be obtained using the equation (2.84) [57]:

$$r_k = \frac{4.15}{\log\left(\frac{p_o}{p}\right)} \tag{2.85}$$

However, r_k is not the actual radius of the pore since condensation process occurs after absorption of one layer on the walls of the pore. Therefore, the actual pore radius, r_p can be expressed as:

$$r_p = r_k + t_a \tag{2.86}$$

Where, t_a is the thickness of the adsorbed film prior to condensation process. For liquid N_2, t_a can be expresses as:

$$t_a = 3.54 \left\{ \frac{5}{\ln\left(\frac{p_o}{p}\right)} \right\}^{\frac{1}{3}} \tag{2.87}$$

The change in volume of adsorbed N_2 gas, ΔV_{gas} is used to calculate the change in volume of adsorbed liquid N_2 as shown below: `

$$\Delta V_{liq} = \frac{\Delta V_{gas}}{22.4 \times 10^3} \times 34.6 = \Delta V_{gas} \times 1.54 \times 10^{-3} \tag{2.88}$$

Hence the cumulative pore volume can be written in terms of actual and Kelvin pore size as given below [58]:

$$V_p = \left(\frac{\overline{r_p}}{\overline{r_k}}\right)^2 \left[\Delta V_{liq} - (\Delta t \Sigma\, S \times 10^{-4})\right] \tag{2.89}$$

Where, S is the surface area of pore and can be written as [58]:

$$S = \frac{2V_p}{\overline{r_p}} \times 10^4 \tag{2.90}$$

The plot between $\overline{r_p}$ along x-axis and $\left(\frac{V_p}{\Delta r_p}\right)$ along y-axis gives the pore size distribution graph. In type IV and type V isotherms, a distinct plateau is observed as presented in Figure 2.15 and hence the single point adsorption at a relative pressure (p/p_o) of 0.95 is used to calculate the total pore volume. This value of relative pressure is chosen since it should be present after the pore condensation stage. The total pore volume can be

obtained by changing the adsorbed amount (W_a) into liquid volume considering that at saturation point, densities of both the adsorbate and bulk liquid (ρ_l) are equal.

The pore volume can be expressed as [57].

$$V_p = \frac{W_a}{\rho_l} \tag{2.91}$$

2.8 References

[1] Bagotsky, V.S., Skundin, A.M. and Volfkovich, Y.M. *Electrochemical power sources: batteries, fuel cells, and supercapacitors*. John Wiley & Son, 2015.

[2] Eftekhari, A. and Fang, B. Electrochemical hydrogen storage: opportunities for fuel storage, batteries, fuel cells, and supercapacitors. *International Journal of Hydrogen Energy*, 42(40):25143-25165, 2017.

[3] Wijeratne, K. *Conducting Polymer Electrodes for Thermogalvanic Cells*. PhD thesis, Department of Science and Technology, Linkö ping University, Sweden, 2019.

[4] Silvester, D.S. *Electrochemical studies in room temperature ionic liquids*. PhD thesis, Department of Chemistry, University of Oxford, 2008.

[5] Kumar, R.V. and Sarakonsri, T., Introduction to electrochemical cells. In High Energy Density Lithium Batteries: Materials, Engineering, Applications, pages 1-25, ISBN:978-3-527-32407-1. WILEY-VCH Verlag GmbH & Co. KGaA, Weinheim, 2010.

[6] Sulaiman, Y., *Characterisation of pedot and its derivatives in electrochemical sensing applications*. PhD thesis, Department of Chemistry, Durham University, 2012.

[7] Borghei, M. Novel carbon nanomaterials for the direct methanol fuel cell electrodes. PhD thesis, Deprtment of Applied Physics, Aalto University, 2015.

[8] Bard, A.J., Faulkner, L.R. and White, H.S. *Electrochemical methods: fundamentals and applications*. John Wiley & Sons, 2nd edition, 2000.

[9] Zhang, L.L. and Zhao, X.S. Carbon-based materials as supercapacitor electrodes. *Chemical Society Reviews*, 38(9):2520-2531, 2009.

[10] Nakamura, M., Sato, N., Hoshi, N. and Sakata, O. Outer Helmholtz plane of the electrical double layer formed at the solid electrode–liquid interface. *ChemPhysChem*, 12(8):1430-1434, 2011.

[11] Ševčík, A. Oscillographic polarography with periodical triangular voltage. *Collection of Czechoslovak Chemical Communications*, 13:349-377, 1948.

[12] Randles, J.E.B. A cathode ray polarograph. *Transactions of the Faraday Society*, 44:322-327, 1948.

[13] Nicholson, R.S. Theory and application of cyclic voltammetry for measurement of electrode reaction kinetics. *Analytical chemistry*, 37(11):1351-1355, 1965.

[14] Elgrishi, N., Rountree, K.J., McCarthy, B.D., Rountree, E.S., Eisenhart, T.T. and Dempsey, J.L. A practical beginner's guide to cyclic voltammetry. *Journal of chemical education*, 95(2):197-206. 2018.

[15] Aristov, N. and Habekost, A. Cyclic voltammetry-A versatile electrochemical method investigating electron transfer processes. *World J. Chem. Educ*, *3*(5):115-119, 2015.

[16] Naylor, P.D. *The electrochemical oxidation of methanol in acid and alkaline fuel cell environments*. PhD thesis, Loughborough University, 1998.

[17] Pickup, P.G., Kuo, K.N. and Murray, R.W. Electrodeposition of metal particles and films by a reducing redox polymer. *Journal of the Electrochemical Society*, 130(11):2205, 1983.

[18] Srinivasan, S. and Gileadi, E. The potential-sweep method: A theoretical analysis. *Electrochimica Acta*, 11(3):321-335, 1966.

[19] Laviron, E.J.J. General expression of the linear potential sweep voltammogram in the case of diffusionless electrochemical systems. *Journal of Electroanalytical Chemistry and Interfacial Electrochemistry*, 101(1):19-28, 1979.

[20] Laviron, E. Adsorption, autoinhibition and autocatalysis in polarography and in linear potential sweep voltammetry. *Journal of Electroanalytical Chemistry and Interfacial Electrochemistry*, 52(3):355-393, 1974.

[21] Laviron, E. A critical study of the factors causing the appearance of Brdička's adsorption currents: Influence of the interactions between the adsorbed molecules. *Journal of Electroanalytical Chemistry and Interfacial Electrochemistry*, 63(3):245-261, 1975.

[22] Laviron, E. Theoretical study of a reversible reaction followed by a chemical reaction in thin layer linear potential sweep voltammetry. *Journal of Electroanalytical Chemistry and Interfacial Electrochemistry*, 39(1), 1-23, 1972.

[23] Laviron, E. Theoretical study of the kinetics of the homogeneous EE electrochemical reaction. *Journal of Electroanalytical Chemistry and Interfacial Electrochemistry*, 148(1):1-16. 1983.

[24] Laviron, E. Theory of regeneration mechanisms in thin layer potential sweep voltammetry. *Journal of Electroanalytical Chemistry and Interfacial Electrochemistry*, 87(1):31-37, 1978.

[25] Wipf, D.O., Kristensen, E.W., Deakin, M.R. and Wightman, R.M. Fast-scan cyclic voltammetry as a method to measure rapid heterogeneous electron-transfer kinetics. *Analytical Chemistry*, 60(4):306-310, 1988.

[26] Heinze, J. Cyclic voltammetry—"electrochemical spectroscopy". New analytical methods (25). Angewandte Chemie International Edition in English, 23(11) 831-847, 1984.

[27] Lemmer, C., Bouvet, M. and Meunier-Prest, R. Proton coupled electron transfer of ubiquinone Q_2 incorporated in a self-assembled monolayer. *Physical Chemistry Chemical Physics*, 13(29):13327-13332, 2011.

[28] Stuckey, P.A., *Kinetic studies and electrochemical processes at fuel cell electrodes.* PhD thesis, Department of Chemical Engineering, Case Western Reserve University, 2011.

[29] Haddox, R.M., 2002. *Electron transfer kinetic studies of 1-electron, 1-proton redox couples attached to electrodes*. PhD thesis, Department of Chemistry, West Virginia University, 2002.

[30] Gabe, D.R. The centenary of Tafel's equation. *Transactions of the IMF*, 83(3):121-124, 2005.

[31] Weber, J. *Aqueous Electrocatalysis in Concentrated Electrolyte Solutions.* PhD thesis, Department of Chemistry, University of Bath, 2016.

[32] Kear, G. and Walsh, F.C. The characteristics of a true Tafel slope. *Corrosion and materials*, 30(6):51-55, 2005.

[33] Kanoun, O. *Impedance Spectroscopy: Advanced Applications: Battery Research, Bioimpedance, System Design*. De Gruyter, 2019.

[34] Delcourt-Lancon, A. *Electrochemical analysis supported by macro and microelectrode array.* PhD thesis, Department of Chemistry, Durham University, 2011.

[35] Mansor, N.B. *Development of catalysts and catalyst supports for polymer electrolyte fuel cells.* PhD thesis, Department of Chemical Engineering, University College London, 2015.

[36] Cesiulis, H.,Tsyntsaru, N., Ramanavicius, A. and Ragoisha, G. The study of thin films by electrochemical impedance spectroscopy. In *Nanostructures and thin films for multifunctional applications*, pages 3-42, ISBN:978-3-319-30197-6. Springer, Cham, 2016.

[37] Macdonald, J.R. and Barsoukov, E. *Impedance spectroscopy: theory, experiment, and applications*. John Wiley & Sons, 2018.

[38] Chang, B.Y. and Park, S.M. Electrochemical impedance spectroscopy. *Annual Review of Analytical Chemistry*, *3*(1):207-229, 2010.

[39] Randles, J.E.B. Kinetics of rapid electrode reactions. *Discussions of the faraday society*, 1:11-19, 1947.

[40] Scholz, F. *Electroanalytical methods*. Springer, Berlin, 2nd edition, 2010.

[41] Malko, D. Electrocatalytic and catalytic oxygen reduction utilising transition metal and heteroatom doped carbon materials. PhD thesis, Department of Chemistry, Imperial College London, 2016.

[42] Jervis, J.R. *Development of Novel Alloy Electrocatalysts for the Hydrogen Oxidation Reaction in Alkaline Media and their Application to Low Temperature Fuel Cells*. PhD thesis, Department of Chemical Engineering, University College London, 2015.

[43] Yoon, D. *Electrochemical studies of Cerium and Uranium in LiCl-KCl eutectic for fundamentals of pyroprocessing technology*. PhD thesis, Department of Mechanical and Nuclear Engineering, Virginia Commonwealth University, 2016.

[44] Sekar, N. and Ramasamy, R.P. Electrochemical impedance spectroscopy for microbial fuel cell characterization. *J Microb Biochem Technol S*, 6(2):1-14, 2013.

[45] Brownson, D.A. and Banks, C.E. Interpreting electrochemistry. In *The handbook of graphene electrochemistry*, pages 23-77, ISBN: 978-1-4471-6427-2. Springer, London, 2014.

[46] Anovitz, L.M. and Cole, D.R. Characterization and analysis of porosity and pore structures. *Reviews in Mineralogy and geochemistry*, 80(1):61-164, 2015.

[47] Lawrence, M. and Jiang, Y. Porosity, pore size distribution, micro-structure. In *Bio-aggregates based building materials*, pages 39-71, Springer, Dordrecht, 2017.

[48] Langmuir, I. The adsorption of gases on plane surfaces of glass, mica and platinum. *Journal of the American Chemical society*, 40(9):1361-1403, 1918.

[49] Cmarik, G.E. *The effects of functionalization on adsorption properties of microporous materials*. PhD thesis, School of Chemical and Biomolecular Engineering, Georgia Institute of Technology, 2014.

[50] Brunauer, S., Deming, L.S., Deming, W.E. and Teller, E. On a theory of the van der Waals adsorption of gases. *Journal of the American Chemical society*, 62(7):1723-1732, 1940.

[51] Sing, K.S. Reporting physisorption data for gas/solid systems with special reference to the determination of surface area and porosity (Recommendations 1984). *Pure and applied chemistry*, 57(4):603-619, 1985.

[52] Butt, H.J., Graf, K. and Kappl, M. *Physics and Chemistry of Interfaces*. Wiley-VCH Verlag GmbH & Co. KGaA*:* Weinheim, 2003.

[53] Rouquerol, J., Rouquerol, F., Llewellyn, P., Maurin, G. and Sing, K.S. *Adsorption by powders and porous solids: principles, methodology and applications*. Academic press, 2013.

[54] Balbuena, P.B. and Gubbins, K.E. Theoretical interpretation of adsorption behavior of simple fluids in slit pores. *Langmuir*, 9(7):1801-1814, 1993.

[55] Sing, K.S. and Williams, R.T. Physisorption hysteresis loops and the characterization of nanoporous materials. *Adsorption Science & Technology*, 22(10):773-782, 2004.

[56] Pierce, C. and Smith, R.N. The Adsorption-Desorption Hysteresis in Relation to Capillarity of Adsorbents. *The Journal of Physical Chemistry*, 54(6):784-794, 1950.

[57] Lowell, S., Shields, J.E., Thomas, M.A. and Thommes, M. *Characterization of porous solids and powders: surface area, pore size and density*. Springer Science & Business Media, 2006.

[58] Barrett, E.P., Joyner, L.G. and Halenda, P.P. The determination of pore volume and area distributions in porous substances. I. Computations from nitrogen isotherms. *Journal of the American Chemical society*, 73(1):373-380, 1951.